

# Intrinsic Zero-Linear and Zero-Area Compressibilities over an Ultrawide Pressure Range within a *Gear-Spring* Structure

Dequan Jiang<sup>1</sup>, Ting Wen<sup>1\*</sup>, Huimin Song<sup>2</sup>, Zimin Jiang<sup>1</sup>, Chen Li<sup>1</sup>, Ke Liu<sup>1</sup>, Wenge Yang<sup>1</sup>, Ho-kwang Mao<sup>1</sup> & Yonggang Wang<sup>1\*</sup>

<sup>1</sup>Center for High Pressure Science and Technology Advanced Research (HPSTAR), Beijing 100094, <sup>2</sup>School of Materials Science and Engineering, Peking University, Beijing 100871

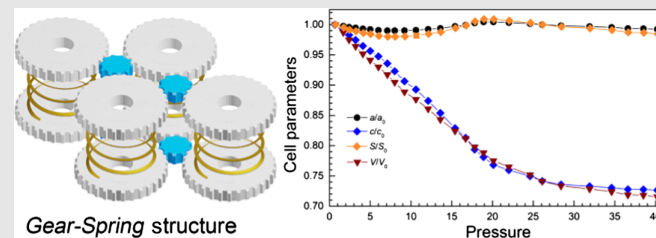
\*Corresponding authors: [ting.wen@hpstar.ac.cn](mailto:ting.wen@hpstar.ac.cn); [yonggang.wang@hpstar.ac.cn](mailto:yonggang.wang@hpstar.ac.cn)

Cite this: CCS Chem. 2022, 4, 3246–3253

DOI: 10.31635/ccschem.022.202101739

Materials with zero-linear compressibility (ZLC) and zero-area compressibility (ZAC) have great promise for specific applications retaining constancy in specific directions or planes under external impaction. To date, no more than 10 ZLC/ZAC materials have been reported, most of which have very limited working pressure ranges (<10 GPa). Herein, we report the observation of ZLC and ZAC in  $\text{Li}_2\text{Ti}(\text{IO}_3)_6$  with a *gear-spring* type structure over an ultrawide pressure range (0–40 GPa). Structural analysis from experimental and theoretical calculations revealed that the rotatable metal coordination polyhedral (gears) and extremely compressible metal chains (springs) work together to form an exquisite mechanical unloading device with intrinsic ZLC and ZAC behavior. Moreover,  $\text{Li}_2\text{Ti}(\text{IO}_3)_6$  set a record-wide ZLC/ZAC working pressure range (up to 40 GPa) among the currently

known anisotropic compression materials. The demonstration of intrinsic and long-lasting ZLC/ZAC with a *gear-spring* mechanism allowed shock-resistant precision optics to be applied under extreme conditions.



**Keywords:** high pressure, zero-linear/zero-area compressibilities, *gear-spring* mechanism, ultrawide pressure range

## Introduction

Substances typically contract under external hydrostatic pressure, just as they expand with heat and contract with cold.<sup>1–3</sup> From a thermodynamics perspective, it is impossible for a given material to exhibit negative volume compressibility.<sup>4</sup> Nevertheless, several material types possess negative compressibility in specific crystalline directions or planes, while the overall cell volume keeps

decreasing under compression.<sup>5–9</sup> In the last decade, materials with negative linear compressibility (NLC) and negative area compressibility (NAC) have been explored widely with specific mechanisms such as *wine-rack*, *honeycomb* networks, and the *lifshitz* model.<sup>10–13</sup> In general, zero-linear compressibility (ZLC) and zero-area compressibility (ZAC) could be achieved readily by finding a balance between negative and positive compressibilities. The linear and area compressibilities of diamond

and Os are used as the standard to classify a ZLC or ZAC material.<sup>14–17</sup> ZLC and ZAC materials are ideal candidates for precision instruments applied under extreme environments such as submarine fiber-optic communication and shock-resistant optical windows.<sup>18,19</sup> Surprisingly, materials with ZLC or ZAC have been rarely discovered compared with those with NLC and NAC properties.<sup>12,14,20–23</sup> Meanwhile, there is no clear structure–property mechanism for the rational design of ZLC/ZAC materials.

In the decade's exploration of materials with abnormal compressibility, remarkable findings have been concentrated in two types of materials: metal–organic frameworks (MOFs) and all-inorganic frameworks.<sup>5</sup> The most important strategy to achieve materials with abnormal compressibility is to establish a clear and instructive structure–property relationship. The diverse organic units endow MOFs with the ability to exhibit flexible mechanical responses under compression,<sup>24–30</sup> including both large NLC and near-ZLC. The *wine-rack* structure model is the most popular mechanism describing the NLC and near-ZLC behaviors in MOFs. Particularly, the “molecular gears and torsion springs” structure model was proposed to describe the NLC and extreme compressibility of  $LnFe(CN)_6$  ( $Ln$  = Ho, Lu, or Y), which benefitted from the  $LnN_6$  torsion springs and the rigid  $Fe(CN)_6$  gears.<sup>31</sup> However, MOFs are soft and usually show the above-mentioned abnormal compressibility within a very narrow pressure range, typically of no more than 10 GPa, which significantly limits their potential applications. Comparatively, all-inorganic frameworks possessing covalently-bonded frameworks are less compressible and include borates. Although the highest pressure of ZLC is 8 GPa, found in  $(Ca,Sr)B_2O_4$  to date, from a structural chemistry viewpoint, they are still good candidates with abnormal compressibility in a relatively wide pressure range.<sup>5</sup> In addition, all-inorganic frameworks could possess good chemical/physical stability and excellent optical performances, making them a potential for next-generation shock-resistant optical windows and fiber communications. Unfortunately, a precise mechanism for the rational design of all-inorganic frameworks with abnormal compressibility is lacking. An exception is the recently reported *Lu-Ban stool* model for  $(Ca,Sr)B_2O_4$ , in which the subtle counterbalance originated from the expansion and contraction effect between the rotation of the  $[BO_3]$  “planks” and the shrinkage of Ca-O “legs” attributed to an excellent ZLC property.<sup>14</sup>

We aimed to explore all-inorganic optical materials with both excellent ZLC/ZAC properties and good chemical/physical stabilities using a structural design strategy. Numerous known inorganic compounds in the inorganic crystal structure database (ICSD) have been screened to search for framework-like structures, among which a unique family of transition metal iodates with metal–metal bonding and chains were identified with potential

for ZLC/ZAC behaviors. Herein, we report the anomalous mechanical responses of  $Li_2Ti(IO_3)_6$  to external pressure as a representative inorganic framework structure. The anisotropic compressibility of  $Li_2Ti(IO_3)_6$  was examined using *in situ* X-ray diffraction (XRD), Raman spectra, and first-principles calculations. A *gear-spring* mechanism was proposed to be responsible for the emerging intrinsic ZLC/ZAC properties, which sheds light on the future structural design of all-inorganic materials with anomalous compressibility.

## Results and Discussion

Phase-pure  $Li_2Ti(IO_3)_6$  was obtained using a hydrothermal method as both white powders and single transparent crystals. At ambient conditions,  $Li_2Ti(IO_3)_6$  crystallized in the hexagonal space group  $P6_3$  with cell parameters of  $a = 9.372(2)$  Å and  $c = 5.113(1)$  Å (*Supporting Information Figure S1*). Figure 1a shows the crystal structure of  $Li_2Ti(IO_3)_6$  consisting of face-sharing  $TiO_6$  chains along the  $c$ -axis, distorted  $IO_3$  units, and  $LiO_6$  octahedra. The structure is noncentrosymmetric with a very strong second-harmonic generation (SHG) efficiency of  $\sim 500$  times  $\alpha$ - $SiO_2$ , comparable with those of  $BaTiO_3$  (400 times  $\alpha$ - $SiO_2$ ) and  $LiNbO_3$  (600 times  $\alpha$ - $SiO_2$ ).<sup>32</sup> Both the  $Ti^{4+}$  and  $I^{5+}$  cations were located within asymmetric coordination environments due to the second-order Jahn-Teller effects. The parallel alignment of the lone pair electrons on the  $I^{5+}$  cations contributed mainly to the macroscopic polarity of  $Li_2Ti(IO_3)_6$  (*Supporting Information Figure S2*).<sup>33,34</sup> Notably, each  $TiO_6$  octahedron linked with six  $IO_3$  polyhedra to form a large anionic  $[(TiO_{6/2})^{2-} \cdot 6(IO_{1/2}O_{2/1})^0]^{2-}$  “cylinder” in the  $ab$  plane; these nano-cylinders were separated by six-coordinated  $Li^+$  cations to achieve charge balance. In such an inorganic framework, the “cylinders” were expected to have the ability to “rotate” around the  $Ti$ - $Ti$  axis since the connection manner between  $(TiO_{6/2})^{2-}$  and six  $(IO_{1/2}O_{2/1})^0$  was corner-sharing. Thus, the anionic  $[(TiO_{6/2})^{2-} \cdot 6(IO_{1/2}O_{2/1})^0]^{2-}$  was considered a rigid “roller.” Previous studies provided preliminary verification of anomalous compressibility of similar metal iodates, such as  $Fe(IO_3)_3$  and  $Zn(IO_3)_2$ .<sup>35,36</sup> Therefore, we have sufficient justification to expect  $Li_2Ti(IO_3)_6$  to have peculiar mechanical responses to external pressure.

*In situ* high-pressure XRD measurements were conducted to study the compressibility of  $Li_2Ti(IO_3)_6$  with the “inorganic-framework” structure (Figure 1b). No obvious structural phase transition was observed under compression up to 40.2 GPa since there was only a peak shift instead of a new peak emerging or disappearing, and the pressure effect on the crystal structure was reversible (*Supporting Information Figure S3*). Different Bragg peaks exhibited distinct shift behaviors under compression, implying extremely anisotropic compressibility along different crystallographic axes. Among them,

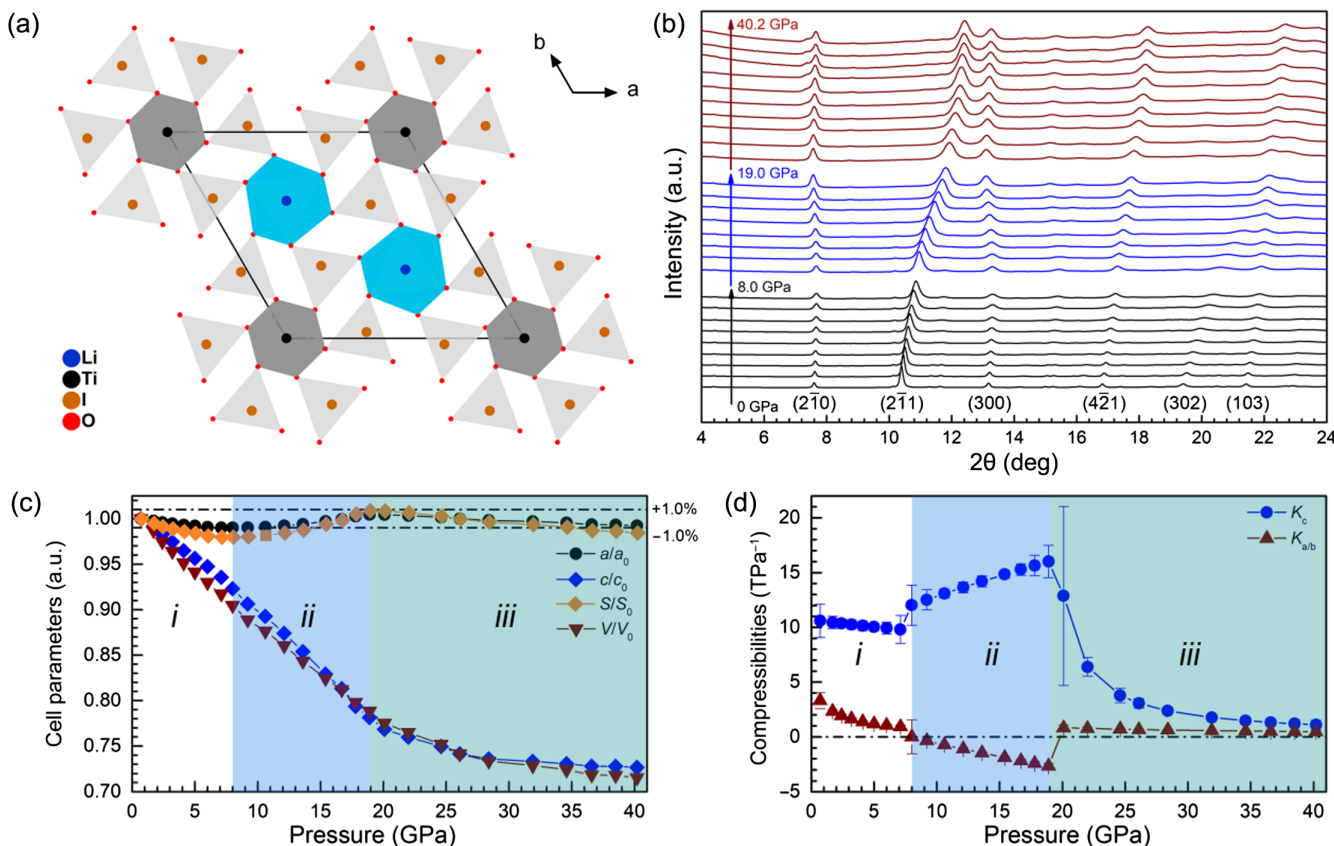


**Figure 1** | Crystal structure and compression behavior of  $\text{Li}_2\text{Ti}(\text{PO}_4)_6$ . (a) Hexagonal structure of  $\text{Li}_2\text{Ti}(\text{PO}_4)_6$  at ambient conditions, consisting of face-sharing  $\text{TiO}_6$  chain (dark gray) along the  $c$  axis, distorted  $\text{IO}_3$  units (light gray), and  $\text{LiO}_6$  octahedra (blue). (b) XRD patterns of  $\text{Li}_2\text{Ti}(\text{PO}_4)_6$  at high pressures. The anisotropic compressibility is evident without a structural phase transition. (c) Cell parameters and volume as pressure functions, showing intrinsic ZLC and ZAC behavior along the  $a/b$  directions and in the  $ab$  plane, respectively. The dotted lines represent the change within a very small range ( $\pm 1\%$ ). (d) Pressure-dependent linear compressibilities ( $K_{a/b}$  and  $K_c$ ) and error bars of  $\text{Li}_2\text{Ti}(\text{PO}_4)_6$  are calculated using the online PASCAL package.<sup>37</sup>

the  $(hk0)$  peaks such as  $(210)$  and  $(300)$  virtually sustained their  $2\theta$  values, indicating incompressibility or minimal compressibility along the  $a$  and  $b$  axes. Specifically, the  $(hk0)$  peaks shifted slightly to the lower  $2\theta$  angle first in the 0–8 GPa range (i), and then slightly to the higher  $2\theta$  angle in the 8–19 GPa (ii), and finally to the lower  $2\theta$  angle again above 19 GPa (iii) (Supporting Information Figure S4). By contrast, the  $(hkl)$  peaks such as  $(211)$  with  $l \neq 0$  shifted quickly to the higher  $2\theta$  angle under compression up to 40 GPa, indicating large compressibility along the  $c$  axis.

Figure 1c shows the refined cell parameters of  $\text{Li}_2\text{Ti}(\text{PO}_4)_6$  as functions of applied pressure (Supporting Information Table S1 and Figures S5 and S6). An extremely anisotropic compression behavior was evident. The evolution of the  $a$  axis underwent three pressure regions in accordance with the peak shift of the  $(hk0)$  planes. Notably, the overall change of the  $a$  axis ( $\Delta a$ ) in the 0–40.2 GPa region was as low as 0.97%, a low enough value to be regarded as ZLC. Due to the hexagonal symmetry of

space group  $P6_3$  with  $a = b$ , the  $ab$  plane exhibited similar compression behavior with individual  $a$  and  $b$  axes, that is, the overall area change of the  $ab$  plane ( $\Delta s$ ) in the 0–40.2 GPa was as low as 1.95%, also low enough value to represent a ZAC. Comparatively, the  $c$  axis exhibited tremendous compressibility with  $\Delta c = 28.69\%$  at 40.2 GPa, and a normal  $V$ - $P$  curve was obtained in the whole pressure range.

The linear compressibility ( $K_l$ ) has been defined previously as  $-dl/dp$  to evaluate the strength of a given material's mechanical response to external pressure.<sup>5</sup> Figure 1d represents the pressure-dependent linear compressibilities ( $K_{a/b}$  and  $K_c$ ) of  $\text{Li}_2\text{Ti}(\text{PO}_4)_6$ , derived using the online PASCAL package<sup>37</sup> and within the three pressure ranges discussed above (i, ii, and iii). It is interesting to observe that  $K_{a/b}$  maintained very small values throughout the whole pressure range: The calculated values for individual pressure ranges were:  $K_a = 1.06 \text{ TPa}^{-1}$  and  $K_c = 10.54 \text{ TPa}^{-1}$  for (i), (0–8 GPa);  $K_a = -1.88 \text{ TPa}^{-1}$  and  $K_c = 14.84 \text{ TPa}^{-1}$  for (ii), (8–19 GPa);  $K_a = 0.58 \text{ TPa}^{-1}$

and  $K_c = 1.78 \text{ TPa}^{-1}$  for (iii), (19–40.2 GPa), respectively ([Supporting Information Figure S7](#)). It was obvious that the  $K_a$  values in regions (i) and (iii) were both small and could be compared to those of diamond ( $0.75 \text{ TPa}^{-1}$ ) and Os ( $0.70 \text{ TPa}^{-1}$ ), which were deemed the standards of ZLC materials. The absolute  $K_a$  value in the region (ii) was more than twice that of diamond and Os and could be deemed NLC. However, this NLC effect was still relatively weak among the reported NLC materials,<sup>5</sup> in which the largest one could achieve  $-76 \text{ TPa}^{-1}$  in  $\text{Ag}_3[\text{Co}(\text{CN})_6]$ .<sup>11</sup> Nevertheless, region (ii) played a significant role in averaging the positive linear compressibility (PLC) in regions (i) and (iii), and thus, achieved a ZLC within the whole pressure region. If we took the (i) + (ii) regions (0–19 GPa) into account, the positive  $K_a$  in range (i) and the negative  $K_a$  in range (ii) yielded a very small overall  $K_a$  value of  $-0.23 \text{ TPa}^{-1}$  in the 0–19 GPa region, still small enough to be characteristic of ZLC. It was necessary to consider the distinct compression properties in both the separate and overall pressure regions for such material with “switching” compressibilities. Thus,  $\text{Li}_2\text{Ti}(\text{IO}_3)_6$  was a promising ZLC material in both the  $a$  and  $b$  directions in the pressure range of 0–40.2 GPa. Of course,  $\text{Li}_2\text{Ti}(\text{IO}_3)_6$  was also a promising ZAC material since the area change of the  $ab$  plane ( $\Delta s$ ) was as low as 1.95% within 0–40.2 GPa.

The online PASCAL package is only applicable to those cases with either a positive or a negative  $K_i$ . To calculate the total  $K_i$  in our case with both positive and negative linear compressibilities in a pressure range, we simply use the most primitive formulas ( $K_i = -\Delta l / \Delta p$  and  $K_s = -\Delta s / s \Delta p$ ) to evaluate the linear and area compressibilities, where  $l$  represented the length of the starting unit cell,  $s$  represented the area of the initial crystal plane,  $\Delta l$ ,  $\Delta s$ , and  $\Delta p$  represented the changes of linear, area, and pressure, respectively. The recalculated  $K_i$  and  $K_s$  in the pressure range of 0–40.2 GPa are provided in [Supporting Information Figure S8](#), and the compressive properties of representative ZLC/ZAC materials, including the *superhard* diamond and Os, used as references, are concluded in Table 1.

First of all,  $\text{Li}_2\text{Ti}(\text{IO}_3)_6$  possessed relatively small  $K_i$  ( $0.24 \text{ TPa}^{-1}$ ) and  $K_s$  ( $0.48 \text{ TPa}^{-1}$ ) within these materials, including diamond ( $K_i = 0.62 \text{ TPa}^{-1}$  and  $K_s = 1.23 \text{ TPa}^{-1}$ ) and Os metal ( $K_i = 0.54/0.60 \text{ TPa}^{-1}$  and  $K_s = 1.02 \text{ TPa}^{-1}$ ), making it worthy of a ZLC and ZAC material. Remarkably, inorganic ceramics or crystalline materials with both ZAC properties and transparency with important wavelengths have rarely been reported, holding a great promise for practical shock-resistant optical usages. Second,  $\text{Li}_2\text{Ti}(\text{IO}_3)_6$  exhibited ZLC and ZAC in an ultrawide pressure range, that is, 0–40.2 GPa, compared with ZLC/ZAC MOFs and metal borates. Although 40.2 GPa might not be the highest pressure value for  $\text{Li}_2\text{Ti}(\text{IO}_3)_6$  to survive, this value still refreshed the world record of ZLC/ZAC material (except diamond and Os). As we already know, there are several structural mechanisms for previously

discovered ZLC/ZAC materials, including *wine-rack* for MOFs, *Lu-Ban stool*, *corrugated graphite*, *lifshitz* for metal borates, and *superhard* for diamond and Os; however,  $\text{Li}_2\text{Ti}(\text{IO}_3)_6$  does not belong to any of these mechanisms.

The crystal structure of  $\text{Li}_2\text{Ti}(\text{IO}_3)_6$  could be regarded vividly as a *gear-spring* type. As shown in Figure 2a, the visualized *gear-spring* model of  $\text{Li}_2\text{Ti}(\text{IO}_3)_6$  comprised of Gear-A (the anionic  $[(\text{TiO}_{6/2})^{2-} \cdot 6(\text{IO}_{1/2}\text{O}_{2/1})^0]^{2-}$ ), Gear-B ( $\text{LiO}_6$  octahedra), and an extremely compressible spring (Ti-Ti distances or  $c$ ), as shown in [Supporting Information Figure S9](#). This model was derived entirely from the real crystal structure and could perfectly describe and explain the ZLC/ZAC phenomena of  $\text{Li}_2\text{Ti}(\text{IO}_3)_6$ .

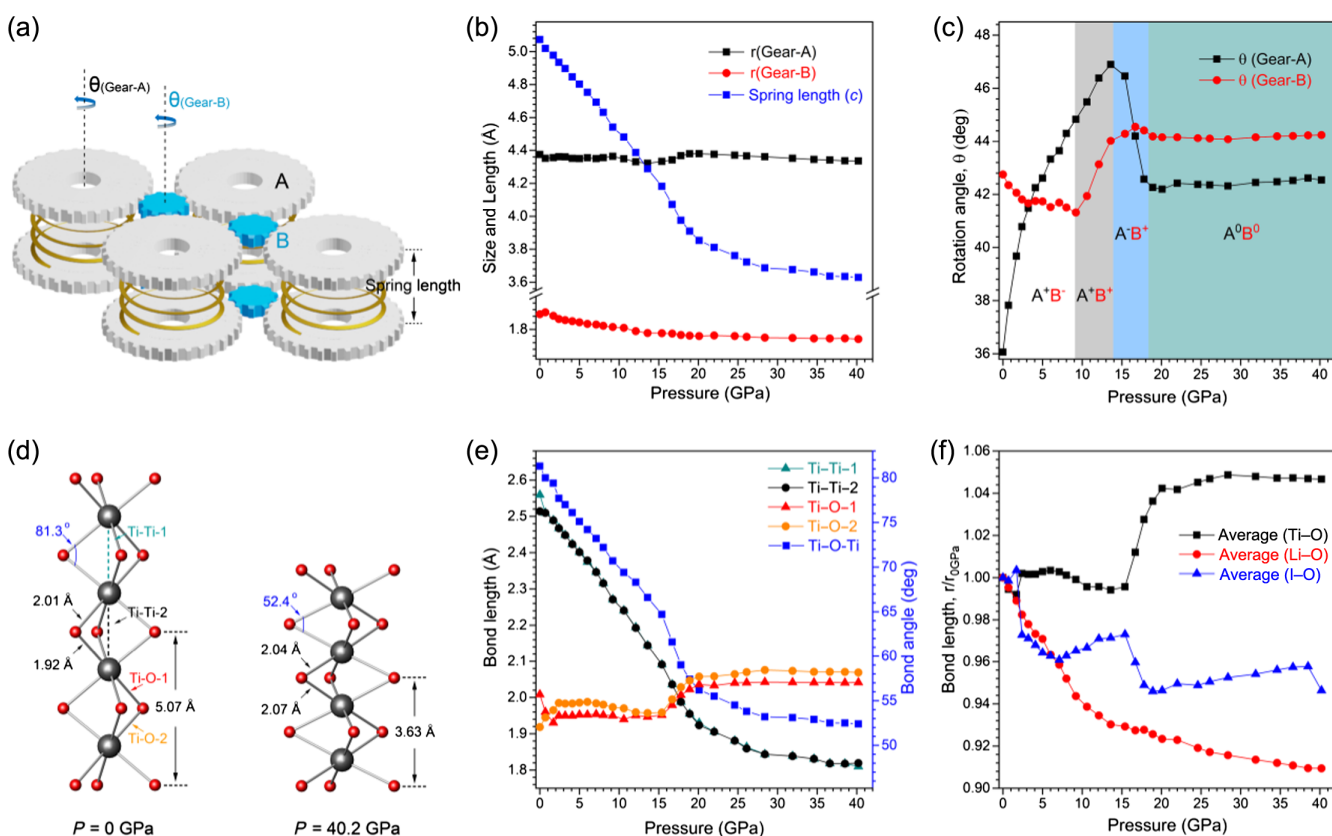
The parameters of the *gear-spring* model, gear radii [ $r$ (Gear-A) and  $r$ (Gear-B)], spring length ( $c$ ) and rotation angles [ $\theta$ (Gear-A), and  $\theta$ (Gear-B)] were derived from structural optimization of first-principles calculation using the experimental cell parameters of  $\text{Li}_2\text{Ti}(\text{IO}_3)_6$  under various pressures. As rigid “gears,” the sizes of “Gear-A” and “Gear-B” essentially remained unchanged, which was validated perfectly by the theoretical calculation results (Figure 2b). In the meantime, the spring length ( $c$ ) decreased rapidly along with an increase in applied pressure, working together as real springs. Amazingly, the two gears (A and B) could rotate synergistically in terms of either direction or angles (Figure 2c). Unlike the previously derived three pressure regions (i, ii, and iii) of the cell parameter evolution, four rotation processes were observed under compression: (i)  $\text{A}^+(\text{counterclockwise})$   $\text{B}^-$  (clockwise) in 0–9 GPa, (ii-a)  $\text{A}^+\text{B}^+$  in 9–14 GPa, (ii-b)  $\text{A}^-\text{B}^+$  in 14–18 GPa, and (iii)  $\text{A}^0\text{B}^0$  in 18–40 GPa, respectively. Thus, it was reasonable to believe that the rotation of the gears could convert the external pressure to the compression direction of the spring.

Figure 2d shows the representative structures of the  $\text{TiO}_6$ -chain at 0 GPa and the highest pressure of 40.2 GPa. The working mechanism of the “spring” was clear from the dramatic changes of the Ti-Ti distances and Ti-O-Ti bond angles. The  $c$  value (spring length) was reduced from 5.07 to 3.63 Å, together with the highly flattened Ti-O-Ti angle (from 81.3° to 52.4°) but almost unchanged Ti-O bondlengths (from 1.92/2.01 to 2.04/2.07 Å). The detailed changes of individual bondlengths during the *gear-spring* working process under compression are displayed in Figures 2e and 2f. Both the Ti-Ti distances and Ti-O-Ti angles exhibited similar changes under compression up to 40 GPa, and there was no distortion from the Ti-O bondlengths within the  $\text{TiO}_6$  octahedra. The average bondlengths of I-O and Ti-O also showed cooperative changes under high pressure to maintain the unchanged size of Gear-A. In brief, the emerging ZLC/ZAC phenomena in  $\text{Li}_2\text{Ti}(\text{IO}_3)_6$  could be explained accurately employing the *gear-spring* mechanism. Materials with such a “gear” and “spring” cooperative structure are expected to have intrinsic ZLC/ZAC properties, also in an ultrawide pressure range.

**Table 1 | The Compressibility and Pressure Range in All Reported ZAC/ZLC Materials**

Material	Mechanism	$K_I$ (TPa $^{-1}$ ) <sup>a</sup>	$K_s$ (TPa $^{-1}$ ) <sup>a</sup>	$P$ (GPa)	References
MIL-122(In)	<i>Wine-rack</i>	0	/	0–10.5	22
[C(NH <sub>2</sub> ) <sub>3</sub> ][Cd(HCOO) <sub>3</sub> ]	<i>Wine-rack</i>	0.75	1.51	0–0.5	21
SrB <sub>2</sub> O <sub>4</sub>	<i>Lu-Ban stool</i>	-0.47	/	0–8.0	14
CaB <sub>2</sub> O <sub>4</sub>	<i>Lu-Ban stool</i>	0.34	/	0–8.1	14
LiBO <sub>2</sub>	<i>Corrugated-graphite</i>	1.54	/	0–2.5	20
RbBe <sub>2</sub> BO <sub>3</sub> F <sub>2</sub>	<i>Lifshitz</i>	0.05	0.1	0–2.6	12
CsBe <sub>2</sub> BO <sub>3</sub> F <sub>2</sub>	<i>Lifshitz</i>	-0.03	-0.07	0–3.2	12
GeO <sub>2</sub>	/	0.08	/	0–8.0	23
Dimond	<i>Superhard</i>	0.62	1.23	0–45.0	15
Os	<i>Superhard</i>	0.60 <sup>a</sup> 0.54 <sup>c</sup>	1.02	0~63.8	17
<b>Li<sub>2</sub>Ti(VO<sub>3</sub>)<sub>6</sub></b>	<b>Gear-spring</b>	<b>1.50</b> <b>-0.13</b> <b>0.24</b>	<b>3.00</b> <b>-0.26</b> <b>0.48</b>	<b>0–8.0</b> <b>0–19.0</b> <b>0–40.2</b>	<b>This work</b>

<sup>a</sup>  $K_I$  and  $K_s$  are calculated by the formulas ( $K_I = -\Delta l/l\Delta p$  and  $K_s = -\Delta s/s\Delta p$ ); <sup>a</sup> and <sup>c</sup> represent the linear compressibilities along the  $a$  and  $c$  direction. The bold values represent that those values are from this work.



**Figure 2 | The Gear-spring mechanism for ZLC/ZAC under compression.** (a) Visualized gear-spring structure of  $\text{Li}_2\text{Ti}(\text{VO}_3)_6$  comprising of Gear-A (the anionic  $[(\text{TiO}_{6/2})^{2-}\cdot 6(\text{VO}_{1/2}\text{O}_{2/1})^0]^{2-}$ ), Gear-B ( $\text{LiO}_6$  octahedra), and the extremely compressible spring-length (Ti-Ti distances or  $c$ ). (b) Evolutions of the size and length of Gear-A, Gear-B, and spring under compression. The “gears” are expected to keep their sizes, and the “springs” are expected to exhibit extremely large compressibility. (c) Pressure-dependent rotations of Gear-A and Gear-B. “+” indicates anticlockwise, and “-” indicates clockwise. (d) Representative structures of the  $\text{TiO}_6^-$  chain at 0 and 40.2 GPa, showing the working mechanism of the “spring.” (e and f) Bond-length and bond-angle evolutions in the gear-spring structure of  $\text{Li}_2\text{Ti}(\text{VO}_3)_6$  under compression.

DOI: 10.31635/ccschem.022.202101739

Citation: CCS Chem. 2022, 4, 3246–3253

Link to VoR: <https://doi.org/10.31635/ccschem.022.202101739>

We probed the local structure evolution of  $\text{Li}_2\text{Ti}(\text{IO}_3)_6$  during the ZLC/ZAC processes by *in situ* high-pressure Raman spectra ([Supporting Information Figure S10](#)). At first, the Raman profile remained largely unchanged under compression, except for gradual shifts of the peaks, indicating the absence of a structural phase transition. The peaks located in the ranges of 400–600 and 600–850  $\text{cm}^{-1}$  could be assigned to the stretching vibration modes of the  $[\text{TiO}_6]$  octahedra and  $[\text{IO}_3]$  pyramids, respectively. The softening of the  $[\text{IO}_3]$  peaks (shifting continuously to a lower wavenumber) indicated an elongation of the I–O bonds.

SHG is a common nonlinear optical phenomenon highly related to a crystal structure symmetry<sup>38–40</sup>; thus, an ideal probe to subtle structure evolution. Our high-pressure SHG experiment indicated that  $\text{Li}_2\text{Ti}(\text{IO}_3)_6$  remained SHG-active up to 40.2 GPa ([Supporting Information Figure S11](#)). It was interesting to find that the trend of SHG intensity was similar to that of the cell parameter  $c$ . The SHG response of  $\text{Li}_2\text{Ti}(\text{IO}_3)_6$  was dominated by a consistent arrangement of lone-pair electrons along the  $c$  axis direction. Therefore, the changing trend of SHG response also reflected the compression trend of cell parameter  $c$  to some extent. The long-lasting SHG functionality combined with intrinsic ZLC/ZAC properties within an ultrawide pressure range made  $\text{Li}_2\text{Ti}(\text{IO}_3)_6$  a unique candidate for optically sensitive devices under extreme conditions.

We envisaged a great potential to explore more ZLC/ZAC materials under the guidance of the as-proposed *gear-spring* mechanism: First, a large family of metal iodates exists with the general formula  $A_2M(\text{IO}_3)_6$  or  $M(\text{IO}_3)_n$ , ( $A$  is a monovalent cation;  $M$  is a transition metal).<sup>35,36</sup> It was easy to find *gear-spring* type isostructures with rigid face-sharing  $MO_6$  chains and flexible  $\text{IO}_3$  linkages similar to hexagonal  $\text{Li}_2\text{Ti}(\text{IO}_3)_6$ . Also, we found it interesting to discuss the relationship between crystal symmetry and anomalous compression behaviors (ZLC/ZAC). Generally, ZLC in  $a = b$  crystalline system (e.g., hexagonal for  $\text{Li}_2\text{Ti}(\text{IO}_3)_6$ ) automatically gives rise to ZAC; therefore, compounds with high crystalline symmetries such as cubic, hexagonal, and tetragonal are preferred candidates for ZAC behavior. Theoretically, ZAC could also be achieved by combining PLC and NLC in an  $a \neq b$  crystalline system (although this has yet to be reported). Second, exploring other *gear-spring* structural types out of iodates was possible. Many face-sharing metal-ligand octahedra could serve as both the springs and the large rigid gears, and small anion groups such as  $[\text{BO}_3]$ ,  $[\text{BO}_4]$ , and  $[\text{PO}_4]$  could be interspersed to make the system flexible and rotatable. An appropriate Van der Waals layered structure was also predicted to exhibit ZAC behavior via the *gear-spring* mechanism. Finally, combining the different mechanisms would undoubtedly accelerate the rational design of more ZLC/ZAC material applicable to an ultrawide pressure range.

DOI: [10.31635/ccschem.022.202101739](https://doi.org/10.31635/ccschem.022.202101739)

Citation: CCS Chem. **2022**, 4, 3246–3253

Link to VoR: <https://doi.org/10.31635/ccschem.022.202101739>

## Conclusions

We report intrinsic ZLC and ZAC properties in an all-inorganic iodate material  $\text{Li}_2\text{Ti}(\text{IO}_3)_6$ . The ultrawide working pressure range (0–40.2 GPa) of  $\text{Li}_2\text{Ti}(\text{IO}_3)_6$  set a record for artificial ZLC or ZAC materials (except diamond and Os). Based on structural analyses, we proposed a promising *gear-spring* mechanism that could perfectly describe and explain the anomalous compression behavior of  $\text{Li}_2\text{Ti}(\text{IO}_3)_6$ . We are confident to predict similar anomalous compression properties (including intrinsic ZLC and ZAC) in compounds with such *gear-spring* structures. Moreover,  $\text{Li}_2\text{Ti}(\text{IO}_3)_6$  maintained its nonlinear optical functionality and ZLC/ZAC behaviors to high pressure, making it promising for special optical devices under extreme environments.

## Supporting Information

Supporting Information is available and includes experimental sections and characterization data.

## Conflict of Interest

There is no conflict of interest to report.

## Preprint Acknowledgement

Research presented in this article was posted on a preprint server prior to publication in CCS Chemistry. The corresponding preprint article can be found using the following link: <https://www.researchsquare.com/article/rs-588081/v1>

## Acknowledgments

This work was supported by the Major Program of the National Natural Science Foundation of China (no. 22090041), the National Natural Science Foundation of China (no. 52073003), and the National Key R&D Program of China (no. 2018YFA0305900). High-pressure XRD data were collected at beamline station 4W2 of Beijing Synchrotron Radiation Facility (BSRF), Beijing, China. The authors thank Freyja O'Toole (HPSTAR) for her help with language editing.

## References

1. Grima, J. N.; Caruana-Gauci, R. Materials that Push Back. *Nat. Mater.* **2012**, *11*, 565–566.
2. Lakes, R. Foam Structures with a Negative Poisson's Ratio. *Science* **1987**, *235*, 1038–1040.
3. Ma, Z.; Li, F.; Zhao, D.; Xiao, G.; Zou, B. Whether or Not Emission of  $\text{Cs}_4\text{PbBr}_6$  Nanocrystals: High-Pressure Experimental Evidence. *CCS Chem.* **2020**, *2*, 71–80.

4. Baughman, R. H.; Stafström, S.; Cui, C.; Dantas, S. O. Materials with Negative Compressibilities in One or More Dimensions. *Science* **1998**, *279*, 1522–1524.
5. Cairns, A. B.; Goodwin, A. L. Negative Linear Compressibility. *Phys. Chem. Chem. Phys.* **2015**, *17*, 20449–20465.
6. Fortes, A. D.; Suard, E.; Knight, K. S. Negative Linear Compressibility and Massive Anisotropic Thermal Expansion in Methanol Monohydrate. *Science* **2011**, *331*, 742–746.
7. Zeng, Q.; Wang, K.; Zou, B. Large Negative Linear Compressibility in InH(BDC)<sub>2</sub> from Framework Hinging. *J. Am. Chem. Soc.* **2017**, *139*, 15648–15651.
8. Cairns, A. B.; Thompson, A. L.; Tucker, M. G.; Haines, J.; Goodwin, A. L. Rational Design of Materials with Extreme Negative Compressibility: Selective Soft-Mode Frustration in KMn[Ag(CN)<sub>2</sub>]<sub>3</sub>. *J. Am. Chem. Soc.* **2012**, *134*, 4454–4456.
9. Qiao, Y.; Wang, K.; Yuan, H.; Yang, K.; Zou, B. Negative Linear Compressibility in Organic Mineral Ammonium Oxalate Monohydrate with Hydrogen Bonding Wine-Rack Motifs. *J. Phys. Chem. Lett.* **2015**, *6*, 2755–2760.
10. Cairns, A. B.; Catafesta, J.; Levelut, C.; Rouquette, J.; Lee, A.; Peters, L.; Thompson, A. L.; Dmitriev, V.; Haines, J.; Goodwin, A. L. Giant Negative Linear Compressibility in Zinc Dicyanoaurate. *Nat. Mater.* **2013**, *12*, 212–216.
11. Goodwin, A. L.; Keen, D. A.; Tucker, M. G. Large Negative Linear Compressibility of Ag<sub>3</sub>[Co(CN)<sub>6</sub>]. *Proc. Natl. Acad. Sci. U. S. A.* **2008**, *105*, 18708–18713.
12. Jiang, X.; Luo, S.; Kang, L.; Gong, P.; Yao, W.; Huang, H.; Li, W.; Huang, R.; Wang, W.; Li, Y.; Li, X.; Wu, X.; Lu, P.; Li, L.; Chen, C.; Lin, Z. Isotropic Negative Area Compressibility over Large Pressure Range in Potassium Beryllium Fluoroborate and its Potential Applications in Deep Ultraviolet Region. *Adv. Mater.* **2015**, *27*, 4851–4857.
13. Hodgson, S. A.; Adamson, J.; Hunt, S. J.; Cliffe, M. J.; Cairns, A. B.; Thompson, A. L.; Tucker, M. G.; Funnella N. P.; Goodwin, A. L. Negative Area Compressibility in Silver(I) Tricyanomethanide. *Chem. Commun.* **2014**, *50*, 5264–5266.
14. Jiang, X.; Yang, Y.; Molokeev, M. S.; Gong, P.; Liang, F.; Wang, S.; Liu, L.; Wu, X.; Li, X.; Li, Y.; Wu, S.; Li, W.; Wu, Y.; Lin, Z. Zero Linear Compressibility in Nondense Borates with a “Lu-Ban Stool”-like Structure. *Adv. Mater.* **2018**, *30*, 1801313.
15. Occelli, F.; Loubeyre P.; LeToullec, R. Properties of Diamond under Hydrostatic Pressures Up to 140 GPa. *Nat. Mater.* **2003**, *2*, 151–154.
16. Cynn, H.; Klepeis, J. E.; Yoo, C. S.; Young, D. A. Osmium Has the Lowest Experimentally Determined Compressibility. *Phys. Rev. Lett.* **2002**, *88*, 135701.
17. Godwal, B. K.; Yan, J.; Clark, S. M.; Jeanloz, R. High-Pressure Behavior of Osmium: An Analog for Iron in Earth’s Core. *J. Appl. Phys.* **2012**, *111*, 112608.
18. Evans, K. E.; Alderson, A. Auxetic Materials: Functional Materials and Structures from Lateral Thinking! *Adv. Mater.* **2000**, *12*, 617–628.
19. Baughman, R. H. Auxetic Materials: Avoiding the Shrink. *Nature* **2003**, *425*, 667.
20. Jiang, X.; Molokeev, M. S.; Dong, L.; Dong, Z.; Wang, N.; Kang, L.; Li, X.; Li, Y.; Tian, C.; Peng, S.; Li, W.; Lin, Z. Anomalous Mechanical Materials Squeezing Three-Dimensional Volume Compressibility into One Dimension. *Nat. Commun.* **2020**, *11*, 5593.
21. Zeng, Q.; Wang, K.; Zou, B. Near Zero Area Compressibility in a Perovskite-like Metal-Organic Frameworks [C(NH<sub>2</sub>)<sub>3</sub>][Cd(HCOO)<sub>3</sub>]. *ACS Appl. Mater. Interfaces* **2018**, *10*, 23481–23484.
22. Yu, Y.; Zeng, Q.; Chen, Y.; Jiang, L.; Wang, K.; Zou, B. Extraordinarily Persistent Zero Linear Compressibility in Metal-Organic Framework MIL-122(Ind). *ACS Materials Lett.* **2020**, *2*, 519–523.
23. Haines, J.; Léger, J. M.; Chateau, C.; Pereira, A. S. Structural Evolution of Rutile-Type and CaCl<sub>2</sub>-Type Germanium Dioxide at High Pressure. *Phys. Chem. Minerals* **2000**, *27*, 575–582.
24. Horike, S.; Shimomura, S.; Kitagawa, S. Soft Porous Crystals. *Nat. Chem.* **2009**, *1*, 695.
25. Ortiz, A. U.; Boutin, A.; Fuchs, A. H.; Coudert, F. X. Anisotropic Elastic Properties of Flexible Metal-Organic Frameworks: How Soft Are Soft Porous Crystals? *Phys. Rev. Lett.* **2012**, *109*, 195502.
26. Mellot-Draznieks, C.; Serre, C.; Surble, S.; Audebrand, N.; Ferey, G. Very Large Swelling in Hybrid Frameworks: A Combined Computational and Powder Diffraction Study. *J. Am. Chem. Soc.* **2005**, *127*, 16273–16278.
27. Maji, T. K.; Matsuda, R.; Kitagawa, S. A Flexible Interpenetrating Coordination Framework with a Bimodal Porous Functionality. *Nat. Mater.* **2007**, *6*, 142–148.
28. Ogborn, J. M.; Collings, I. E.; Moggach, S. A.; Thompson, A. L.; Goodwin, A. L. Supramolecular Mechanics in a Metal-Organic Framework. *Chem. Sci.* **2012**, *3*, 3011–3017.
29. Zeng, Q.; Wang, K.; Qiao, Y.; Li, X.; Zou, B. Negative Linear Compressibility due to Layer Sliding in a Layered Metal–Organic Framework. *J. Phys. Chem. Lett.* **2017**, *8*, 1436–1441.
30. Zeng, Q.; Wang, K.; Zou, B. Negative Linear Compressibility Response to Pressure in Multitype Wine-Rack Metal–Organic Frameworks. *ACS Materials Lett.* **2020**, *2*, 291–295.
31. Duyker, S. G.; Peterson, V. K.; Kearley, G. J.; Studer, A. J.; Kepert, C. J. Extreme Compressibility in LnFe(CN)<sub>6</sub> Coordination Framework Materials via Molecular Gears and Torsion Springs. *Nat. Chem.* **2016**, *8*, 270–275.
32. Chang, H.-Y.; Kim, S.-H.; Halasyamani, P. S.; Ok, K. M. Alignment of Lone Pairs in a New Polar Material: Synthesis, Characterization, and Functional Properties of Li<sub>2</sub>Ti(IO<sub>3</sub>)<sub>6</sub>. *J. Am. Chem. Soc.* **2009**, *131*, 2426–2427.
33. Hu, C.-L.; Mao, J.-G. Recent Advances on Second-Order NLO Materials Based on Metal Iodates. *Coord. Chem. Rev.* **2015**, *288*, 1–17.
34. Chen, J.; Hu, C.-L.; Mao, F.-F.; Yang, B.-P.; Zhang, X.-H.; Mao, J.-G. REI<sub>5</sub>O<sub>14</sub> (RE=Y and Gd): Promising SHG Materials Featuring the Semicircle-Shaped I<sub>5</sub>O<sub>14</sub><sup>3-</sup> Polyiodate Anion. *Angew. Chem. Int. Ed.* **2019**, *58*, 11666–11669.
35. Liang, A.; Rahman, S.; Saqib, H.; Rodriguez-Hernandez, P.; Muñoz, A.; Nébert, G.; Yousef, I.; Popescu, C.; Errandonea,

- D. First-Order Isostructural Phase Transition Induced by High Pressure in  $\text{Fe}(\text{IO}_3)_3$ . *J. Phys. Chem. C* **2020**, *124*, 8669–8679.
36. Liang, A.; Popescu, C.; Manjon, F. J.; Rodriguez-Hernandez, P.; Muñoz, A.; Hebboul, Z.; Errandonea, D. Structural and Vibrational Study of  $\text{Zn}(\text{IO}_3)_2$  Combining High-Pressure Experiments and Density-Functional Theory. *Phys. Rev. B* **2021**, *103*, 054102.
37. Cliffe, M. J.; Goodwin, A. L. PASCal: A Principal Axis Strain Calculator for Thermal Expansion and Compressibility Determination. *J. Appl. Cryst.* **2012**, *45*, 1321–1329.
38. Franken, P. A.; Hill, A. E.; Peters, C. W.; Weinreich, G. Generation of Optical Harmonics. *Phys. Rev. Lett.* **1961**, *7*, 118–119.
39. Gong, P.; Liang, F.; Kang, L.; Chen, X.; Qin, J.; Wu, Y.; Lin, Z. Recent Advances and Future Perspectives on Infrared Nonlinear Optical Metal Halides. *Coordin. Chem. Rev.* **2019**, *380*, 83–102.
40. Li, Y.; Yin, C.; Yang, X.; Kuang, X.; Chen, J.; He, L.; Ding, Q.; Zhao, S.; Hong, M.; Luo, J. A Nonlinear Optical Switchable Sulfate of Ultrawide Bandgap. *CCS Chem.* **2020**, *2*, 2298–2306.